

# The fabrication and characterization of PbTiO<sub>3</sub> nanomesas realized on nanostructured SrRuO<sub>3</sub>/SrTiO<sub>3</sub> templates

C C You<sup>1</sup>, R Takahashi<sup>1,3</sup>, A Borg<sup>2</sup>, J K Grepstad<sup>1</sup> and T Tybell<sup>1</sup>

<sup>1</sup> Department of Electronics and Telecommunications, Norwegian University of Science and Technology, 7491 Trondheim, Norway

<sup>2</sup> Department of Physics, Norwegian University of Science and Technology, 7491 Trondheim, Norway

E-mail: [thomas.tybell@iet.ntnu.no](mailto:thomas.tybell@iet.ntnu.no)

Received 9 March 2009, in final form 23 April 2009

Published 3 June 2009

Online at [stacks.iop.org/Nano/20/255705](http://stacks.iop.org/Nano/20/255705)

## Abstract

We report the fabrication of PbTiO<sub>3</sub> nanomesas down to 30 nm lateral size and 4 nm high on nanostructured SrRuO<sub>3</sub>/SrTiO<sub>3</sub> templates by off-axis radio frequency magnetron sputtering. The templates were prepared using a top-down lithography approach based on scanning tunneling microscopy. The growth rate of the PbTiO<sub>3</sub> nanomesas was found to decrease with increasing growth temperature as well as with shrinking template size. Piezoresponse force microscopy measurements for the PbTiO<sub>3</sub> nanomesas showed a strong increase in response with decreasing lateral size. A decrease of the coercive voltage was also observed for the same lateral size range. This laterally size-dependent behavior is attributed to reduction of in-plane strain, when shrinking the nanomesa lateral dimensions.

(Some figures in this article are in colour only in the electronic version)

## 1. Introduction

Ferroelectric perovskite oxides possess functional properties, such as piezoelectricity, pyroelectricity, and ferroelectricity, which makes them interesting for a variety of applications, for example in sensors, actuators, surface acoustic wave filters, electro-optic modulators, and non-volatile random access memories [1–5]. With the aim of incorporating such materials in future nanoelectronic devices, there has been a tremendous effort to understand how size affects material properties at the nanometer length scale [6–13]. Establishing the influence of film thickness on the ferroelectric polarization has been the target of a number of investigations [7–10]. Recently, it was shown that ferroelectricity can be sustained in ultrathin films. For example, PbTiO<sub>3</sub> (PTO) films, with thicknesses down to 1.2 nm, were found to be ferroelectric [9]. For many envisaged devices, effects from a small lateral size may also be important. According to recent theoretical findings [13], the ferroelectric phase transitions in zero-dimensional Pb(Zr, Ti)O<sub>3</sub> (PZT)

nanostructures, with a diameter of ~8 nm and a height of ~6 nm, differ greatly from those of bulk ferroelectrics. This is attributed to the presence of a toroidal moment formed by electric dipole vortices.

In order to investigate ferroelectrics at the smallest length scale, it is important to develop suitable techniques for definition of nanoscale ferroelectric capacitor structures. Physical downscaling can be achieved by top-down approaches based on electron beam lithography (EBL) [14–16] and focused ion beam milling [17, 18], and by bottom-up approaches using self-assembly, self-patterning [19–21] or fabrication techniques which utilize shadow masks [22, 23]. Ferroelectric Pt/PZT/Pt capacitors of ~60 nm lateral size and 20–40 nm high were grown using pulsed laser deposition with anodic aluminum oxide masks [23], while ferroelectric PTO nanograins down to ~20 nm in lateral size and ~6 nm high were achieved by deposition from chemical solution [20]. Investigation of the physical properties of such nanostructures revealed that the piezoelectric properties are strongly dependent on size. A prominent increase in the piezoelectric response was observed for 200 nm thick PZT nanostructures with decreasing lateral size from 200 to

<sup>3</sup> Present address: Department of Materials Science and Engineering, University of Maryland, College Park, MD 20742, USA.

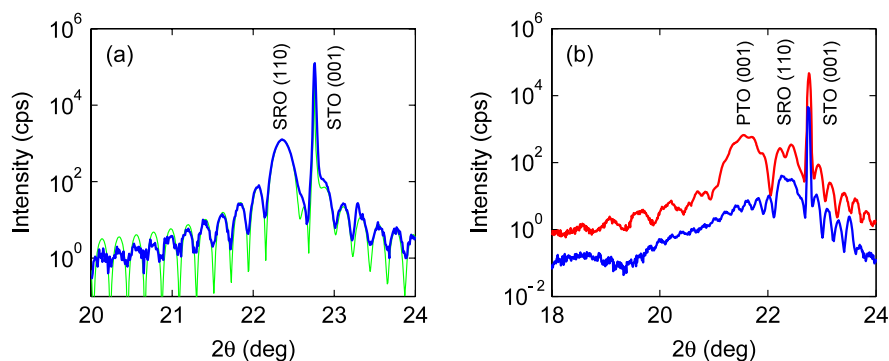


**Figure 1.** (a)  $\theta$ - $2\theta$  diffractogram of the SRO (110) reflection for a 42 nm thick film. The additional satellite peaks (oscillation fringes) allow for precise measurement of the film thickness as indicated by the green fine curve. (b)  $\theta$ - $2\theta$  diffractograms taken around the PTO (001) reflection for a 16 nm thick (upper red curve) and a 4 nm thick (lower blue curve) film deposited on an SRO thin film. Note that the measured intensity of the 4 nm thick sample is offset by an order of magnitude relative to that of the 16 nm thick sample.

100 nm [15], whereas the response was significantly decreased when the lateral size of 100 nm thick PZT cells was reduced from 1  $\mu\text{m}$  to 100 nm [14]. These findings underline the importance of developing novel nanostructuring techniques, which offer the capability of defining high quality and defect-free ferroelectric structures of nanoscale dimensions, so as to facilitate experimental investigations of size effects.

Alternative methods for nanostructuring based on scanning probes have recently attracted attention due to their high lateral resolution [24–28]. In particular, scanning tunneling microscopy (STM) was successfully employed for nanoscale surface modifications of perovskite oxides and to provide a lateral line resolution as small as 3 nm [27]. In a previous study [28], we have shown that nanoscale surface structures can be routinely etched in SrRuO<sub>3</sub> (SRO) thin films by such STM lithography. Here, we report on such top-down nanostructuring of SRO thin films by STM, to form templates for subsequent growth of PTO nanomesas by magnetron sputter deposition. These PTO nanomesas had a lateral size and thickness down to 30 and 4 nm, respectively. This approach offers the possibility of controlling the nanomesa geometry, which is highly desirable for investigation of physical properties of nanostructured ferroelectrics. The present fabrication technique also provides opportunities for construction of device structures from other technically important perovskite oxides such as multiferroics, manganites, and high- $T_c$  superconductors. Moreover, we discuss how substrate temperature and template size affect the growth of PTO nanomesas, as well as the dependence of the piezoelectric response and coercive voltage on the nanomesa lateral size.

## 2. Experimental details

SRO thin films of  $\sim 35$ – $50$  nm thickness were deposited on as-received, (001) oriented single-crystalline SrTiO<sub>3</sub> (STO) substrates by off-axis radio frequency magnetron sputtering. The films were grown at substrate temperatures ranging from  $\sim 590$  to  $690^\circ\text{C}$  in a 100 mTorr atmosphere of oxygen and argon ( $\text{O}_2:\text{Ar} = 4:10$ ).<sup>4</sup> Nanoscale templates were defined

<sup>4</sup> The substrate temperature was typically measured at the center of the substrate, using an optical pyrometer at wavelength 1.5  $\mu\text{m}$  with the emissivity set at 0.7.

in the SRO thin films by employing a commercial ambient STM system equipped with mechanically cut Pt/Ir tips. The STM was operated in constant current mode, and the feedback was on for both etching and imaging. For normal imaging, a positive bias voltage of typically 500 mV and a tunneling current of 300 pA were used. In order to pattern a rectangular template, four lines were etched consecutively by scanning the tip over a preselected area. Typically, we used a bias voltage of 2.8 V, a set-point tunneling current of 40–60 pA, a scan speed of 300 nm s<sup>-1</sup>, and 200–300 scan repetitions per line. Further details can be found elsewhere [28]. A series of templates with lateral size ranging from  $\sim 30$  to 260 nm were prepared. PTO thin films with thicknesses  $\sim 3$ – $16$  nm were subsequently grown on the nanostructured SRO thin film templates by rf magnetron sputtering, in order to obtain the PTO nanomesas. The PTO films were deposited at a substrate temperature of  $\sim 500$ – $530^\circ\text{C}$  in a mixed ambient of oxygen and argon ( $\text{O}_2:\text{Ar} = 4:10$ ) with an overall pressure of 165 mTorr.

To analyze the crystalline properties of the PTO and SRO thin films, x-ray diffraction (XRD) measurements were carried out using a Bruker D8 Discover diffractometer. XRD analysis revealed single-crystalline epitaxial growth of the SRO thin films. Figure 1(a) shows a typical  $\theta$ - $2\theta$  diffractogram of SRO grown on STO substrate, with clearly defined finite thickness oscillation fringes. The SRO film thickness was determined at 42 nm by numerical fitting to the measured oscillation fringes [29], as shown by the green fine curve. Rocking curves measured around the (110) Bragg reflection displayed a full width at half-maximum of typically  $0.02^\circ$ – $0.03^\circ$ , similar to that of the (001) STO substrate reflection. Figure 1(b) reports  $\theta$ - $2\theta$  diffractograms taken for the (001) reflection of 16 nm thick (upper red curve) and 4 nm thick (lower blue curve) PTO films grown on SRO. Note that the thickness fringe of the SRO layer is superimposed on the PTO signal. The XRD data set indicates  $c$ -axis oriented growth of a tetragonal PTO film. Rocking curves taken around the (001) Bragg peak showed a mosaic spread of less than  $0.03^\circ$  for the 16 nm thick film of PTO. Figure 2 displays  $\phi$ -scans of the PTO (101), SRO (112), and STO (101) reflections for a PTO (16 nm)/SRO (39 nm)/STO sample. The fourfold symmetry apparent in the azimuthal scans is evidence of epitaxial growth for both PTO and SRO.

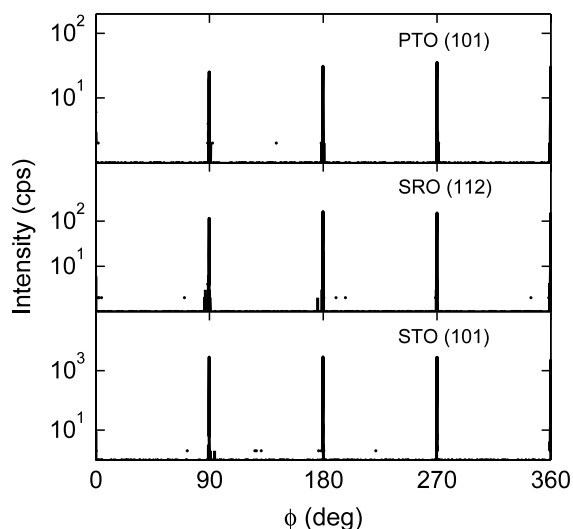


**Figure 2.**  $\phi$ -scans of the PTO (101), SRO (112), and STO (101) reflections recorded for a 16 nm thick PTO film grown on SRO/STO.

The surface morphology of the PTO, SRO, and STO layers was examined with tapping mode atomic force microscopy (AFM). Figure 3(a) shows a representative  $2 \times 2 \mu\text{m}^2$  AFM topography scan of the SRO thin film surface. The SRO surface consists of a well-defined step and terrace structure, similar to that of the STO substrate. Such atomically smooth surfaces are a key prerequisite for successful and reproducible STM nanostructuring. Figures 3(b) and (c) show  $2 \times 2 \mu\text{m}^2$  AFM topography scans of the 16 and 4 nm thick films of PTO on SRO, respectively. The step and terrace surface structure is preserved, similar to that of the SRO thin film and STO substrate surfaces.

In order to carry out local nanoscale AFM investigations, markers were etched in the STO substrates prior to the subsequent film deposition, using a commercial RAITH Elphy Plus EBL system. To prepare these markers, a  $\sim 2 \mu\text{m}$  thick layer of PMMA (polymethylmethacrylate) resist was spun onto the STO substrate. Markers with a linewidth of  $8 \mu\text{m}$  were subsequently written using an electron beam with an accelerating voltage of 20 kV, a probe current of 120–130 pA, and an area dose of  $260 \mu\text{A cm}^{-2}$ . After resist development, the markers were defined in the STO substrate by argon ion etching. Residual PMMA was removed by annealing at  $950^\circ\text{C}$  for 1 h in an oxygen gas flow. The markers obtained could be readily located using the optical positioning system of the AFM.

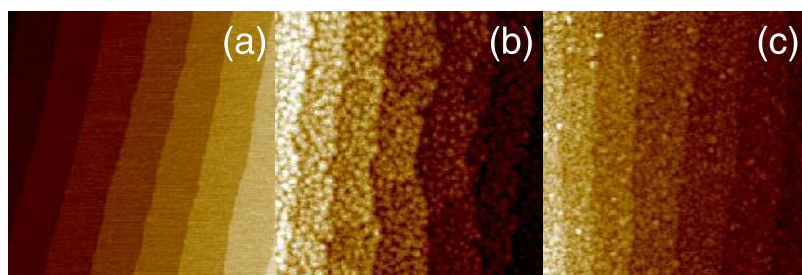


**Figure 3.** (a) Typical AFM topography image of the SRO thin film surface. AFM topography images of (b) 16 nm and (c) 4 nm thick PTO films grown on SRO. The scan size is  $2 \times 2 \mu\text{m}^2$  for all three images.

In order to investigate the piezoelectric properties of the PTO thin films and nanomesas, both piezoresponse force microscopy (PFM) imaging and local hysteresis measurements were performed using a commercial Multimode V AFM equipped with an internal lock-in amplifier system and a signal access module [7, 30]. All PFM measurements were performed in air and at room temperature. Conductive Pt/Ir-coated Si tips were used as a mobile top electrode<sup>5</sup>. For imaging, an ac bias voltage of amplitude 1 V and modulation frequency 10 kHz was applied between the conductive scanning tip and the SRO film, which served as a bottom electrode. In order to probe the local piezoelectric hysteresis properties, a dc bias voltage was superimposed on the tip ac bias voltage, while the amplitude and phase signals were continuously recorded. The amplitude is a measure of the local effective piezoelectric coefficient  $d_{33}$ , and the phase reflects the direction of polarization in the film underneath the tip. In our epitaxial thin films of tetragonal PTO, the two equivalent polarization states were aligned parallel to the growth direction, i.e. perpendicular to the film surface [31, 32]. A dc bias voltage sweep of  $\pm 2$  V was employed for PTO continuous films and nanomesas alike, based on a 16 nm thick PTO sample, while  $\pm 1$  V was sufficient to switch the nanomesas defined for a 4 nm thick PTO sample. An estimate of the piezoelectricity was obtained from the saturation regions of the piezoresponse hysteresis loops, using average amplitudes acquired from bias voltages of  $\pm(1.9\text{--}2)$  V (all continuous films and nanomesas obtained from the 16 nm thick PTO sample) and  $\pm(0.9\text{--}1)$  V (nanomesas obtained from the 4 nm thick PTO sample)<sup>6</sup>.

### 3. Results and discussion

The STM topography images in figures 4(a) and (d) show typical SRO templates with average lateral sizes of  $\sim 65$  and  $\sim 175$  nm, respectively. The AFM images in figures 4(b)

<sup>5</sup> We note that of the two different batches of AFM tips that were used here, one was found to yield a systematically higher piezoelectric amplitude than the other under exactly the same experimental conditions. Force curve measurements showed force constants of typically  $\sim 2.5$  and  $4.5 \text{ N m}^{-1}$  for the two batches. As a result, each amplitude data set was obtained with tips from the same batch. The amplitude data set shown in figures 9 and 10(b) for the 16 nm thick PTO sample was obtained using tips from the batch with force constant  $4.5 \text{ N m}^{-1}$ ; otherwise tips from the batch with force constant  $2.5 \text{ N m}^{-1}$  were employed.

<sup>6</sup> The observed trend of increasing piezoelectricity upon shrinking the lateral dimensions was found to be independent of the region of the saturated hysteresis loop that was used for this analysis, e.g.  $\pm(1.6\text{--}2)$  V and  $\pm(0.6\text{--}1)$  V.

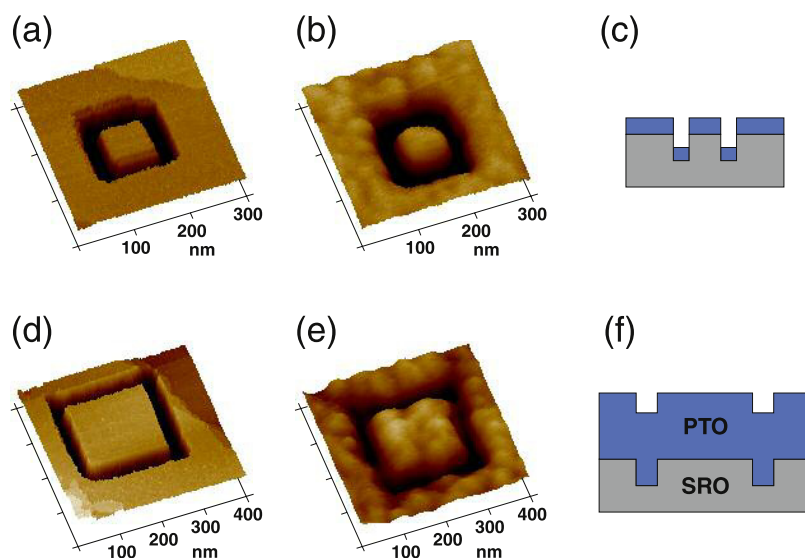


**Figure 4.** STM topography images (a) and (d) show two representative templates defined in the SRO thin film surface by STM lithography. AFM topography images of the PTO nanomesas obtained after (b) 4 nm and (e) 16 nm thick PTO film depositions on these SRO templates as shown in (a) and (d). The ideal growth of PTO on a nanostructured SRO template is illustrated for the 4 nm thick (c) and the 16 nm thick (f) depositions, respectively.

and (e) show the resulting topography after deposition of 4 and 16 nm thick PTO films. The average lateral sizes of these PTO nanomesas are  $\sim 60$  and  $\sim 160$  nm. The average depth of the etched trenches surrounding the SRO template was estimated at  $\sim 4$ – $6$  nm. This suggests that for PTO film thicknesses less than the depth of the trenches, which outline the SRO template, it is possible to form isolated islands of PTO, as illustrated in figure 4(c). For film thicknesses exceeding the depth of the trenches, the template surface topography is preserved at the PTO surface, as is evident from comparison of figures 4(d) and (e) and schematically illustrated in figure 4(f). Hence, the proposed fabrication scheme for physical deposition on nanoscale templates can be used to define free standing islands as well as preparing nanostructured surfaces in thick homogeneous films.

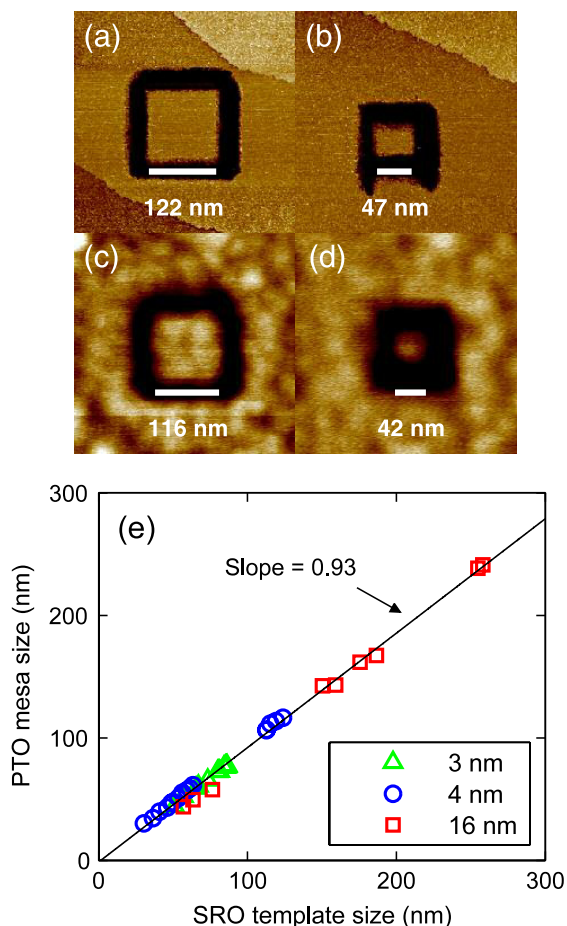
Figure 5 depicts STM topography scans of two SRO templates with lateral sizes (a) 122 nm and (b) 47 nm, respectively. Figures 5(c) and (d) show AFM scans of the PTO nanomesas on these SRO templates after deposition of 4 nm PTO. The lateral size of these PTO nanomesas was estimated at 116 and 42 nm in (c) and (d), respectively. The width of the PTO nanomesa is always found to be smaller than that of the corresponding SRO growth template. The correlation between the average lateral size of the PTO nanomesas and their corresponding SRO templates is displayed in figure 5(e) for 3, 4 and 16 nm thick PTO samples. The solid line in this figure is a linear fit to the data, with a slope of 0.93. This indicates that the lateral size of the PTO nanomesa is in general  $\sim 5$ – $10\%$  smaller than that of the SRO template.

Figure 6(a) shows an AFM line scan across a PTO nanomesa. As can be seen, the height of the nanomesa is lower than that of the surrounding thin film. In figure 6(b), this difference in height,  $\Delta h$ , is plotted versus the average lateral size of the nanomesas for the 3, 4 and 16 nm thick PTO films grown at a substrate temperature of 515 °C. A distinct increase

in  $\Delta h$  was observed upon shrinking the lateral size below  $\sim 50$  nm. Surface height differences up to  $\Delta h \sim 1$  nm were measured for the smallest nanomesas. Figure 6(c) displays  $\Delta h$  versus substrate temperature during growth<sup>7</sup>. The height difference was found to increase at substrate temperatures above 530 °C, which suggests that the PTO growth rate on the SRO template is reduced accordingly. The measured dependence of  $\Delta h$  on the lateral size and substrate temperature indicates that the growth rate of the PTO nanomesas is affected by the adatom surface diffusion. It has been previously shown that the adatom diffusivity increases with increasing growth temperature for similar deposition techniques [33, 34]. It is possible for adatoms arriving within a diffusion length of the template edges to migrate directly into the trenches of the SRO template, thereby effectively reducing the total number of atoms available for formation of the PTO nanomesa. Since the surface diffusion length increases with increasing growth temperature [33], more adatoms can diffuse into the STM-etched trenches, thus resulting in a lower growth rate for the PTO nanomesa. Similarly, when the size of the template is reduced, a larger proportion of adatoms may be expected to migrate to the trenches, thus contributing to the observed increase in  $\Delta h$  with decreasing template dimensions, shown in figure 6(b). Moreover, such growth scenarios are also in agreement with the observations from figure 5, in which the size of the PTO nanomesas was found to be smaller than that of the corresponding SRO templates.

In order to establish a reference level for the PTO nanomesas, piezoresponse hysteresis loop measurements were performed on continuous films. Figure 7 shows the dependence of the piezoelectric amplitude on the PTO film thickness. The

<sup>7</sup> The PTO nanomesas used for the temperature data analysis are taken from three different  $\sim 4$  nm thick PTO samples with the average lateral sizes of the nanomesas being  $\sim 30$ – $50$  nm.

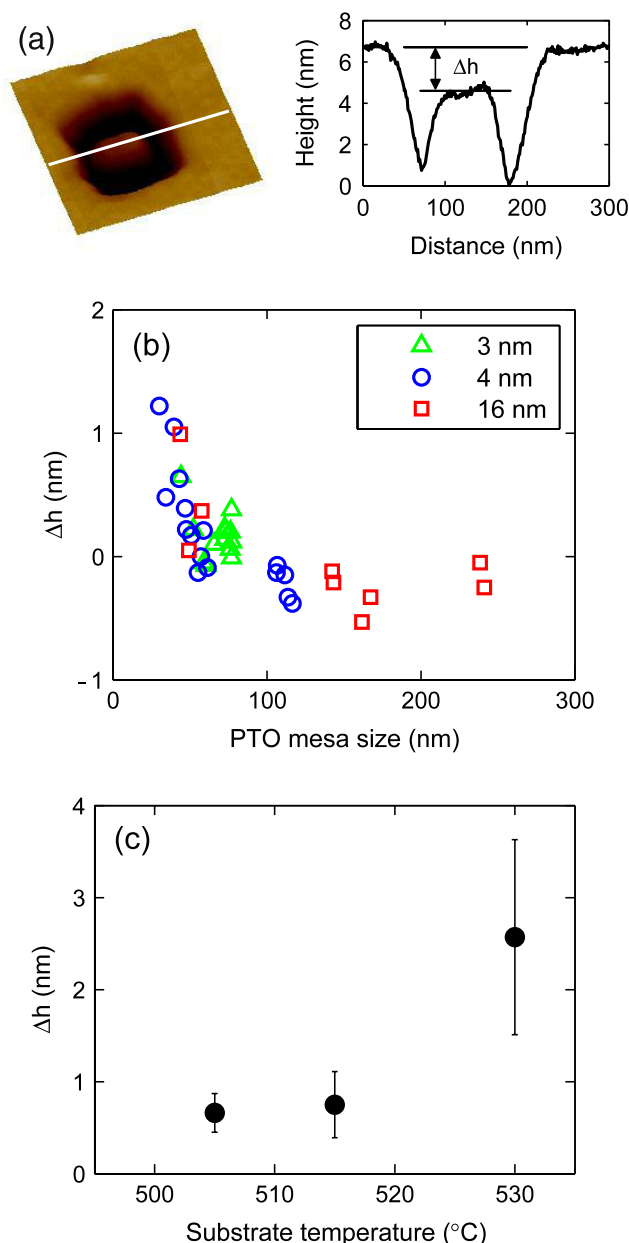


**Figure 5.** STM topography images of two templates with lateral sizes (a) 122 nm and (b) 47 nm, as defined by STM lithography in the SRO thin film. AFM topography measurements of the PTO nanomesas with lateral sizes (c) 116 nm and (d) 42 nm, grown on the SRO templates shown in (a) and (b) for 4 nm PTO deposition. (e) Average lateral size of the PTO nanomesas versus the SRO growth templates. The PTO nanomesas were obtained from 3, 4 and 16 nm thick PTO films. The solid line is a linear fit to the data, with a slope of 0.93.

amplitude was found to drop gradually with decreasing film thickness from 16 to 4 nm, as was previously reported [7, 11]. We note that no piezoresponse hysteresis loop could be obtained for the  $\sim 3$  nm thick film in this study, as the measured signal dropped below the noise level of the PFM measurements.

Figure 8(a) shows a PFM topography scan of a pristine nanomesa with an average lateral size of  $\sim 50$  nm defined in a 4 nm thick PTO sample. Figures 8(b) and (c) show the amplitude and phase of the piezoresponse, measured for the PTO nanomesa. In the amplitude image, an increased amplitude is observed for the PTO nanomesa. Such an increase of the piezoelectric amplitude was also found close to the trenches right across from the nanomesa<sup>8</sup>.  $3 \times 3 \mu\text{m}^2$  PFM scans revealed that these PTO thin film regions with increased piezoresponse are typically confined within an area of up to  $\sim 200$  nm from the trenches. In addition, the piezoelectric

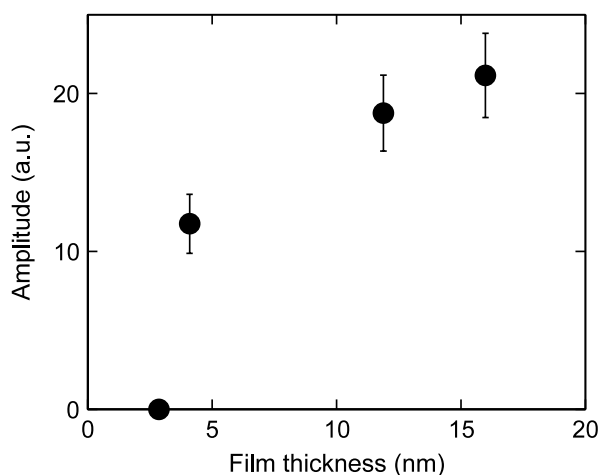
<sup>8</sup> The maximum amplitude level measured for the surrounding film was for certain structures larger than that measured for the PTO nanomesa.



**Figure 6.** (a) Left: AFM topography image of a PTO nanomesa. Right: a cross-section profile along the center of the nanomesa surface, displaying a height difference,  $\Delta h$ , between the nanomesa surface and the surrounding film. (b) The height difference,  $\Delta h$ , versus the average lateral size of PTO nanomesas defined in 3, 4 and 16 nm thick PTO samples. (c) The dependence of  $\Delta h$  on the substrate temperature. The data set is obtained from PTO nanomesas of average lateral size  $\sim 30$ – $50$  nm, defined in three different  $\sim 4$  nm thick PTO samples.

amplitude decreased markedly as the tip was scanned across the trenches.

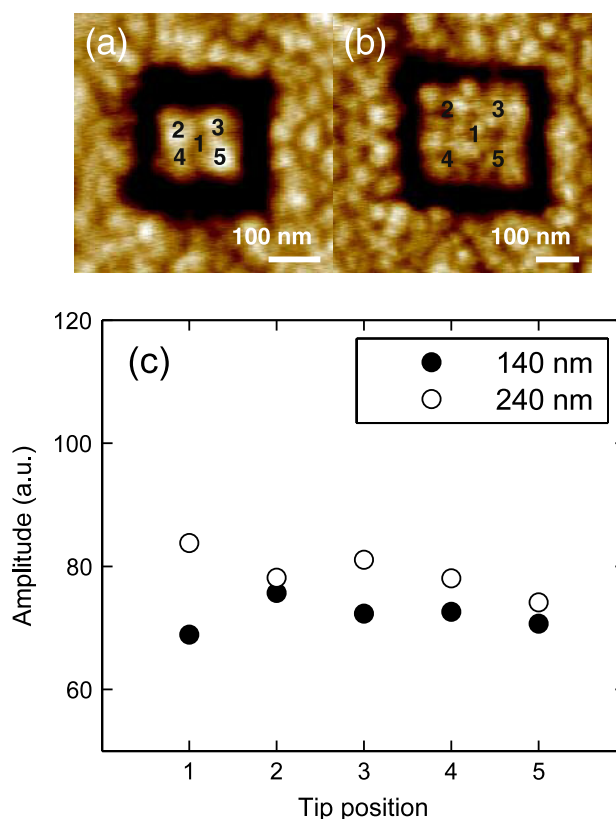
The AFM scans in figures 9(a) and (b) depict two PTO nanomesas defined in a 16 nm thick PTO sample, with average lateral sizes of  $\sim 140$  and  $\sim 240$  nm, respectively. The numbers 1–5 denote the various tip positions for the piezoelectric hysteresis loop measurements. The average piezoelectric amplitude showed little variation with the tip measurement position for both PTO nanomesas (figure 9(c)), suggesting



**Figure 7.** The dependence of the piezoelectric amplitude on the PTO film thickness. Note that the 3, 4 and 16 nm thick PTO films were grown on nanostructured SRO thin films.

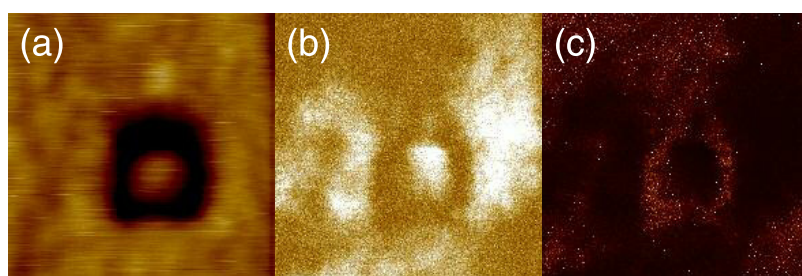
that the piezoelectric response is homogeneous across the nanomesas.

Figure 10(a) shows piezoresponse hysteresis loops recorded for two PTO nanomesas in a 4 nm thick sample with average lateral sizes of  $\sim 30$  and  $\sim 115$  nm, respectively. As can be seen, the measured piezoelectric amplitude is strongly enhanced for the smaller nanomesa compared to that of the larger. Figure 10(b) displays the piezoelectric amplitude as a function of average lateral size for nanomesas defined in both 4 and 16 nm thick PTO samples. In this chart, the piezoelectric amplitude of the nanomesas is normalized with respect to the average amplitude measured for the continuous films. The error bars indicate the standard deviation, as calculated from hysteresis loops obtained with different tips, including different measurement positions on the nanomesa surface. For the nanomesas defined in the 4 nm thick PTO sample, the piezoelectric amplitude increases sharply with decreasing lateral size. For lateral dimensions below  $\sim 60$  nm, it is shown that the piezoelectric amplitude is up to  $\sim 3$  times larger than that of the continuous film. It was previously reported for 200 nm thick PZT structures that the piezoelectric response increased when the structure was scaled down from 200 to 100 nm in lateral dimensions [15]. The present study confirms this trend, even for the smallest PTO nanomesas ( $30 \times 30 \times 4$  nm<sup>3</sup>). According to recent work [16, 35] the



**Figure 9.** AFM topography images of PTO nanomesas defined in a 16 nm thick PTO sample with average lateral sizes (a) 140 nm and (b) 240 nm, respectively. The numbers denote the tip measurement positions. (c) Variation of the average piezoelectric amplitude with tip position for the two PTO nanomesas shown in (a) and (b).

strain state in island nanostructures was found to be dependent on the aspect ratio of the nanostructure. For aspect ratios below 20 the in-plane strain is reduced compared to that of a continuous film [16]. Furthermore, the in-plane strain relaxation is most pronounced in the regions near the edges and corners and lowest in the center of the island, indicating that the clamping conditions are not uniform over the nanomesas. In the present study, the aspect ratio ranges from  $\sim 7$  to 30 for the nanomesas in the 4 nm thick PTO film, indicating a strong increase of average strain relaxation as the dimension is reduced below 50 nm. AFM tips with a nominal tip radius of curvature of 20–25 nm, and a tip–surface contact force



**Figure 8.** (a) PFM topography image of a pristine nanomesa defined in a 4 nm thick PTO sample. (b) Amplitude image revealing an increased piezoresponse for the nanomesa and the adjacent film region. (c) Phase image of the nanomesa. The scan size is  $400 \times 400$  nm<sup>2</sup> for all three images.

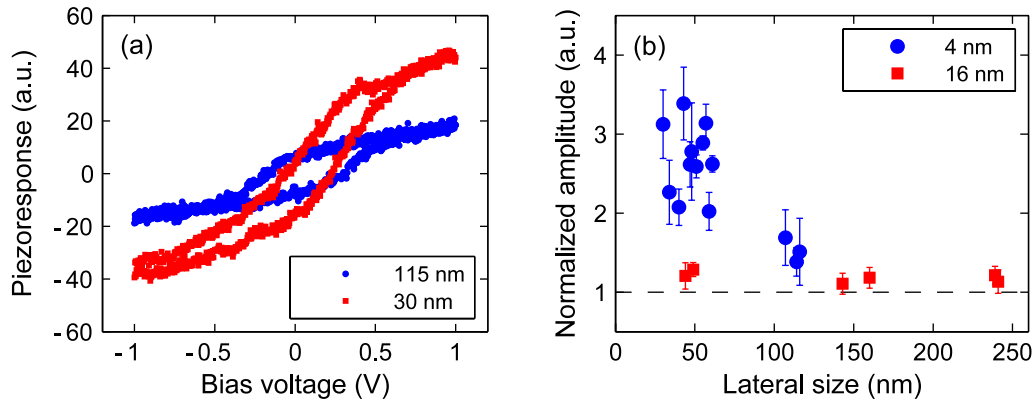


**Figure 10.** (a) Piezoresponse hysteresis loops recorded from nanomesas defined in a 4 nm thick PTO sample showing increased piezoresponse with decreasing lateral size. (b) Normalized piezoelectric amplitude as a function of the average lateral size for nanomesas obtained from 4 and 16 nm thick PTO samples. The dashed line indicates the reference piezoelectric amplitude obtained for a continuous film.

of  $\sim 200$  nN, as derived from the force curve measurements, were used in the PFM measurements. Hence, the PFM measurements were carried out in the strong indentation regime [36]. In this regime, the electric field distribution inside the ferroelectric is predominantly determined by the tip–surface contact area [36, 37], enabling us to measure a true electromechanical response of the ferroelectric material underneath the tip. We note that there might also be a small contribution from the field distribution outside the contact area to the piezoelectric signal. It has been shown that the normal component of the electric field drops rapidly along the radial direction, reaching  $\sim 1/3$  of the value at the tip apex at a distance corresponding to one tip radius [38]. As a result, the entire mesa structure is believed to contribute to the signal for nanomesas below 50–60 nm, the lateral size below which an appreciable reduction of in-plane strain is expected. Hence, we interpret the measured increase in piezoelectric amplitude as a result of the decrease of average in-plane strain upon shrinking the dimensions of the nanomesas [15, 18, 39, 40]. As the in-plane strain is reduced, the nanomesas may expand and contract more freely in lateral directions due to the electromechanical response determined by the piezoelectric coefficient  $d_{31}$ . This response is otherwise impeded by clamping of the continuous film to the substrate [41].

Figure 10(b) also reports that the measured piezoelectric amplitude does not vary significantly with nanomesa lateral size for the 16 nm thick PTO sample. This finding can be understood in terms of the contribution from the continuous PTO film under the nanomesa mounds, as illustrated in figure 4(f). However, it should be noted that the piezoelectric amplitude obtained from these nanomesas is still up to  $\sim 30\%$  larger compared to that of the continuous film, presumably a result of the unclamped edges and sidewalls in the upper section of the nanomesas.

The dependence of the measured coercive voltage on the lateral size is shown in figure 11, where  $\Delta V_c$  is plotted versus average lateral size of the PTO nanomesa for a 4 nm thick sample.  $\Delta V_c = V_c^+ - V_c^-$ , as derived from piezoresponse hysteresis loops, and is averaged over data obtained from different tip measurement positions and normalized to the

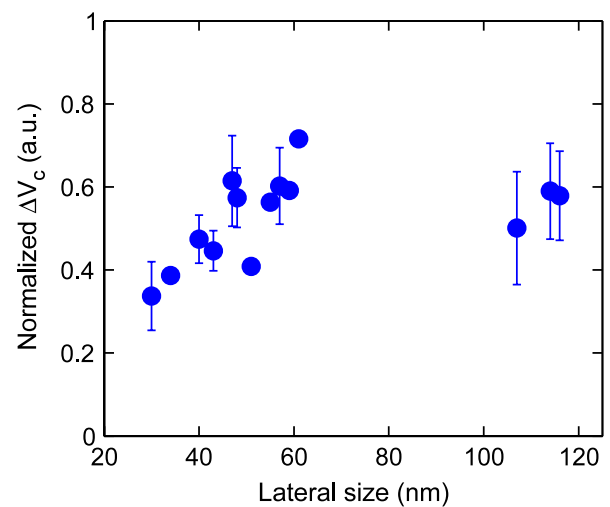


**Figure 11.** Normalized  $\Delta V_c$  as a function of the average lateral size of the PTO nanomesas, as obtained from the 4 nm thick PTO sample.  $\Delta V_c$  is defined as the difference between the positive and negative coercive voltages, i.e.  $\Delta V_c = V_c^+ - V_c^-$ . Here  $\Delta V_c$  is normalized to the average  $\Delta V_c$  measured for the continuous film.

average  $\Delta V_c$  for a continuous film.  $\Delta V_c$  was found to be nearly constant, at  $\sim 0.6$  of the bulk  $\Delta V_c$  value, for lateral sizes above  $\sim 50$  nm, with appreciable reduction for lateral dimensions below  $\sim 50$  nm. We note that for nanomesas smaller than  $\sim 160$  nm lateral size in the 16 nm thick sample,  $\Delta V_c$  is  $\sim 0.5$  of the bulk  $\Delta V_c$  value. In figure 11, the rapid decrease in  $\Delta V_c$  appears in the same lateral size range for which a large increase in the piezoelectric amplitude was observed. For all lateral sizes,  $\Delta V_c$  was found to be  $\sim 2$ – $3$  times lower than that of a continuous film. It has been previously verified both experimentally and theoretically that the coercive field is dependent on strain for homogeneous ferroelectric thin films [42–45]. For strain-relaxed thin films, the energy barrier for domain nucleation is reduced, leading to a lower coercive field [44, 45]. As discussed above, when the nanomesa lateral size decreases, the in-plane strain is reduced due to relaxation at the free surfaces, including sidewalls [16, 46]. Hence, the present data set supports a scenario where the

observed decrease of  $\Delta V_c$  is due to strain relaxation in the PTO nanomesas, when their lateral size is diminished.

#### 4. Conclusions

We have developed a new technique for definition of ferroelectric nanostructures with lateral sizes down to a few tens of nanometers. This technique should in principle allow even smaller structures to be defined by carefully choosing STM nanostructuring parameters, template materials, and physical growth conditions. It also provides the possibility of maintaining nanostructured surfaces in thick homogeneous films. Moreover, the present approach should be suitable for definition of nanomesas in other material classes, such as superconductors, ferromagnets, and dielectrics, which allows probing of their physical properties at nanometer dimensions in a controlled fashion. We have shown that the piezoelectric response of 4 nm high PTO nanomesas increases with decreasing lateral size down to 30 nm. The coercive voltage of these PTO nanomesas was found to decrease with reduced lateral size.

#### Acknowledgments

The authors wish to thank the Research Council of Norway for funding via contract No. 162874/V30, and the NANOMAT nationally coordinated project 'Oxides for Future Information and Communication Technology', contract No. 158518/431.

#### References

- [1] Lines M E and Glass A M 1979 *Principles and Applications of Ferroelectrics and Related Materials* (Oxford: Clarendon)
- [2] Ahn C H, Rabe K M and Triscone J-M 2004 *Science* **303** 488
- [3] Scott J F 2007 *Science* **315** 954
- [4] Sarin Kumar A K, Paruch P, Triscone J-M, Daniau W, Ballandras S, Pellegrino L, Marré D and Tybell T 2004 *Appl. Phys. Lett.* **85** 1757
- [5] Wessels B W 2007 *Annu. Rev. Mater. Res.* **37** 659
- [6] Li S, Eastman J A, Li Z, Foster C M, Newnham R E and Cross L E 1996 *Phys. Lett. A* **212** 341
- [7] Tybell T, Ahn C H and Triscone J-M 1999 *Appl. Phys. Lett.* **75** 856
- [8] Junquera J and Ghosez P 2003 *Nature* **422** 506
- [9] Fong D D, Stephenson G B, Streiffer S K, Eastman J A, Auciello O, Fuoss P H and Thompson C 2004 *Science* **304** 1650
- [10] Lichtensteiger C, Triscone J-M, Junquera J and Ghosez P 2005 *Phys. Rev. Lett.* **94** 047603
- [11] Nagarajan V et al 2006 *J. Appl. Phys.* **100** 051609
- [12] Tybell T, Paruch P, Giamarchi T and Triscone J-M 2002 *Phys. Rev. Lett.* **89** 097601
- [13] Naumov I I, Bellaiche L and Fu H 2004 *Nature* **432** 737
- [14] Alexe M, Harnagea C, Hesse D and Gösele U 1999 *Appl. Phys. Lett.* **75** 1793
- [15] Bühlmann S, Dwir B, Baborowski J and Murali P 2002 *Appl. Phys. Lett.* **80** 3195
- [16] Lee K, Yi H, Park W-H, Kim Y K and Baik S 2006 *J. Appl. Phys.* **100** 051615
- [17] Ganpule C S, Stanishevsky A, Su Q, Aggarwal S, Melngailis J, Williams E and Ramesh R 1999 *Appl. Phys. Lett.* **75** 409
- [18] Nagarajan V, Roytburd A, Stanishevsky A, Prasertchoung S, Zhao T, Chen L, Melngailis J, Auciello O and Ramesh R 2003 *Nat. Mater.* **2** 43
- [19] Chu M-W, Szafraniak I, Scholz R, Harnagea C, Hesse D, Alexe M and Gösele U 2004 *Nat. Mater.* **3** 87
- [20] Rüdiger A, Schneller T, Roelofs A, Tiedke S, Schmitz T and Waser R 2005 *Appl. Phys. A* **80** 1247
- [21] Nonomura H, Nagata M, Fujisawa H, Shimizu M, Niu H and Honda K 2005 *Appl. Phys. Lett.* **86** 163106
- [22] Shin H-J, Choi J H, Yang H J, Park Y D, Kuk Y and Kang C-J 2005 *Appl. Phys. Lett.* **87** 113114
- [23] Lee W, Han H, Lotnyk A, Schubert M A, Senz S, Alexe M, Hesse D, Baik S and Gösele U 2008 *Nat. Nanotechnol.* **3** 402
- [24] Kobayashi A, Grey F, Williams R S and Aono M 1993 *Science* **259** 1724
- [25] Pellegrino L, Bellingeri E, Siri A S and Marré D 2005 *Appl. Phys. Lett.* **87** 064102
- [26] Kim R H, Ahn W S, Han S H and Choi S K 2007 *Appl. Phys. Lett.* **90** 172907
- [27] Bertsche G, Clauss W and Kern D P 1996 *Appl. Phys. Lett.* **68** 3632
- [28] You C C, Rystad N V, Borg A and Tybell T 2007 *Appl. Surf. Sci.* **253** 4704
- [29] Thompson C, Foster C M, Eastman J A and Stephenson G B 1997 *Appl. Phys. Lett.* **71** 3516
- [30] Gruverman A and Kholkin A 2006 *Rep. Prog. Phys.* **69** 2443
- [31] Dahl Ø, Grepstad J K and Tybell T 2008 *J. Appl. Phys.* **103** 114112
- [32] Takahashi R, Dahl Ø, Eberg E, Grepstad J K and Tybell T 2008 *J. Appl. Phys.* **104** 064109
- [33] Neave J H, Dobson P J, Joyce B A and Zhang J 1985 *Appl. Phys. Lett.* **47** 100
- [34] Rijnders G, Blank D H A, Choi J and Eom C-B 2004 *Appl. Phys. Lett.* **84** 505
- [35] Nagarajan V 2005 *Appl. Phys. Lett.* **87** 242905
- [36] Kalinin S V and Bonnell D A 2002 *Phys. Rev. B* **65** 125408
- [37] Kalinin S V, Karapetian E and Kachanov M 2004 *Phys. Rev. B* **70** 184101
- [38] Scrymgeour D A and Hsu J W P 2008 *Appl. Phys. Lett.* **93** 233114
- [39] Roytburd A L, Alpay S P, Nagarajan V, Ganpule C S, Aggarwal S, Williams E D and Ramesh R 2000 *Phys. Rev. Lett.* **85** 190
- [40] Li J-H, Chen L, Nagarajan V, Ramesh R and Roytburd A L 2004 *Appl. Phys. Lett.* **84** 2626
- [41] Lefki K and Dormans G J M 1994 *J. Appl. Phys.* **76** 1764
- [42] Pertsev N A, Rodríguez Contreras J, Kukhar V G, Hermanns B, Kohlstedt H and Waser R 2003 *Appl. Phys. Lett.* **83** 3356
- [43] Choi K J et al 2004 *Science* **306** 1005
- [44] Choudhury S, Li Y L, Chen L Q and Jia Q X 2008 *Appl. Phys. Lett.* **92** 142907
- [45] Paul J, Nishimatsu T, Kawazoe Y and Waghmare U V 2008 *Appl. Phys. Lett.* **93** 242905
- [46] Zhang J X, Wu R, Choudhury S, Li Y L, Hu S Y and Chen L Q 2008 *Appl. Phys. Lett.* **92** 122906